Eur. Phys. J. C 27, 547–553 (2003)
Digital Object Identifier (DOI) 10.1140/epjc/s2003-01153-1

THE EUROPEAN PHYSICAL JOURNAL C

Inclusive production of antihyperons in nC-interactions

The EXCHARM Collaboration

A.N. Aleev, V.P. Balandin, E.A. Goudzovski, D.K. Guriev, P. Hristov, I.M. Ivanchenko, Z.M. Ivanchenko, M.N. Kapishin, N.N. Karpenko, V.D. Kekelidze, Z.I. Kozhenkova, V.V. Koren'kov, I.G. Kosarev, N.A. Kuzmin, A.L. Lyubimov, D.T. Madigojine, V.G. Mazny, A.S. Mestvirishvili, N.A. Molokanova, A.N. Morozov, Yu.K. Potrebenikov, L.A. Slepets, V.N. Spaskov, G.T. Tatishvili, V.V. Trofimov, I.P. Yudin, A.I. Zinchenko
Joint Institute for Nuclear Research, Dubna, Russia

A.P. Bugorski
Institute of High Energy Physics, Protvino, Russia

A.A. Loktionov
Institute of Physics and Technology, Alma-Ata, Kazakhstan

T. Ponta, T. Preda
Institute of Atomic Physics, Bucharest, Romania

I.M. Geshkov
Institute for Nuclear Research and Nuclear Energy, Sofia, Bulgaria

N.S. Amaglobeli, M.V. Kopadze, R.A. Kvatadze, N.L. Lomidze
High Energy Physics Institute, Tbilisi State University, Georgia

T.S. Grigalashvili
Institute of Physics, Georgian Academy of Sciences, Tbilisi, Georgia

Received: 7 June 2002 / Revised version: 23 January 2003 /
Published online: 3 March 2003 –

Abstract. The inclusive production cross-sections of $\bar{\Lambda}^0$, $\bar{\Xi}^+$, and $\bar{\Sigma}(1385)^{\pm}$ in neutron-carbon interactions at ~ 51 GeV mean energy of neutrons have been measured. The parameters n and b of differential cross-section parametrisation $(1-|x_F|)^n \cdot \exp(-bp_t^2)$, where x_F is the Feynman variable, p_t is the transverse momentum, have been obtained. The kinematic region of validity of the parametrisation has been defined. Results are compared with published experimental data.

1 Introduction

The behaviour of differential cross-sections for inclusive production of antihyperons in nucleon-nucleon interactions is poorly explored. The kinematic region of validity of existing theoretical models is also uncertain.

Most of the data on antihyperon production have been obtained in charged kaon beams, as cross-sections of antihyperon production by strange particles are higher than those by nucleons. Some measurements have been performed in proton beams [1–14], and only few in neutron beams [15,16]. The existing data have very large uncertainties. So it is still an open question whether total and differential cross-sections of antihyperon production by protons and neutrons are similar.

In this paper the results on inclusive antihyperon production in neutron-carbon interactions at mean neutron energy ∼51 GeV are presented. The results have been obtained in EXCHARM experiment carried out at the Serpukhov accelerator.

Antihyperons have been identified by their decays:

$$\bar{\Lambda}^0 \to \bar{p}\pi^+, \tag{1}$$

$$\bar{\Xi}^+ \to \bar{\Lambda}^0\pi^+ \hookrightarrow \bar{p}\pi^+, \tag{2}$$

$$\bar{\Sigma}(1385)^{\pm} \to \bar{\Lambda}^0\pi^{\pm} \hookrightarrow \bar{p}\pi^+. \tag{3}$$

2 The EXCHARM experiment

The EXCHARM setup is installed in the neutron beam (channel 5N) of the Serpukhov accelerator. Beam neutrons are produced on the internal beryllium target by 70 GeV primary protons at an angle of zero degrees to the proton orbit. The target is followed by a set of collimators and a lead filter for γ rejection of remotely controlled thickness up to 20 cm. Charged particles are swept out of the beam by accelerator magnets and a special sweeping magnet SP-129 installed at the exit of the final collimator. The

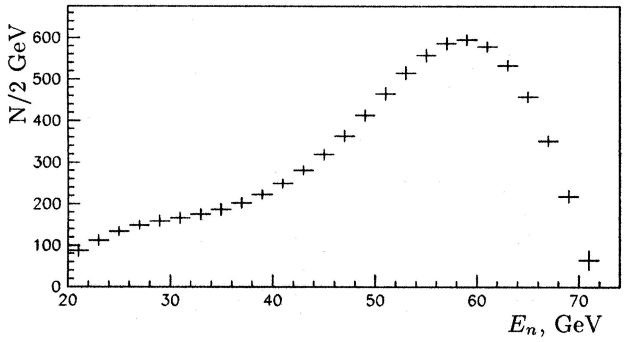

Fig. 1. Neutron beam energy spectrum

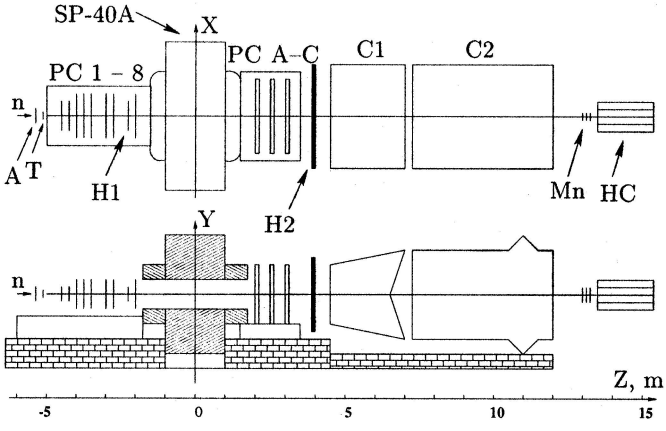

Fig. 2. The EXCHARM spectrometer

neutron energy [17] ranges from 20 GeV to 70 GeV. The mean energy of the beam is $\sim$ 51 GeV (Fig. 1).

The layout of the EXCHARM setup is presented in Fig. 2. The detector is described in the right coordinate system with OZ axis directed along the neutron beam, and OY axis directed vertically up. The centre of coordinate system coincides with the centre of the analysing dipole magnet SP-40A. The magnet aperture is 274×49 cm^2. The magnetic field is directed along the OY axis, and has maximum value of $\approx$ 0.79 T. The polarity of the field was alternated every 5–6 hours during the data taking. The magnet causes a transverse momentum kick of $\approx$ 0.45 GeV/c.

Neutrons are interacting with the 1.3 g/cm^2 (1.5 cm) long carbon target (T) located in front of the spectrometer. Produced charged particles are detected by 11 proportional chambers (PC) with 2 mm wire spacing. Eight chambers upstream the magnet (PC 1–8) have two coordinate planes each. Two of these PC's have wire orientation $\pm 22.5^\circ$ with respect to vertical plane, the others have horizontal and vertical wire orientation. Three chambers downstream of the magnet (PC A–C) have three coordinate planes each. The wire orientations of the three planes are horizontal, vertical and -22.5° with respect to the vertical plane. The charged track momentum resolution of the spectrometer is $\sigma_p/p = 10^{-3} \cdot \sqrt{0.65 \cdot p^2 + 34.55}$, where p is expressed in GeV/c.

Two scintillator hodoscopes $H1$ and $H2$ consisting of 15 and 60 counters, respectively, are used to form the trigger signal. Two multichannel threshold gas Cherenkov counters $C1$ and $C2$ filled with freon and air, respectively, under atmospheric pressure, are intended to separate charged hadrons ($p(\bar{p})$, $K^\pm$, $\pi^\pm$).

The trigger was designed as a coincidence of signals from the hodoscopes $H1$ and $H2$, hodoscopic strips of three PC planes, and an anti-counter A located upstream the target. Trigger requirements selected events with at least four charged particles passing through the spectrometer.

A more detailed description of the apparatus can be found elsewhere [18].

3 Event selection

The presented results are based on the analysis of $\sim$1.84$\times 10^8$ recorded nC-interactions. Experimental events have been processed by the BISON program [19] to reconstruct tracks of charged particles and to define their parameters. To select the events with a particular topology and to perform physical and statistical analysis, the program BISMXC [20] was implemented.

3.1 $\bar{\Lambda}^0$ selection

$\bar{\Lambda}^0$'s are selected by their decay (1) which corresponds to the so called neutral vertex topology. A neutral vertex consists of a pair of oppositely charged reconstructed tracks. The closest distance of approach (CDA) of these tracks should not exceed 0.5 cm (5 standard deviations), which excludes $\sim$17% of all the possible candidates. To reduce the background caused by interactions in the target, the Z coordinate of the decay vertex $Z_{\bar{\Lambda}}$ is required to be in the region situated at a distance at least 10 cm downstream the target:

$$Z_{\bar{\Lambda}} - \left(Z_T + \frac{1}{2} L_T \right) > 10 \text{ cm}, \qquad (4)$$

where $Z_T = -460$ cm is the coordinate of the target centre, and $L_T = 1.5$ cm is the target thickness. The criterion has been selected to minimise the relative error of the number of events in the signal. This condition decreases background by a factor of ~ 2 while removing only $\sim 10\%$ of the signal.

The lower limit of probability of the antiproton hypothesis for the negatively charged track calculated on the basis of the Cherenkov detector data is chosen in order to exclude unambiguously identified π^- and K^-, which allows to decrease the background by a factor of ~ 11.5 removing only $\sim 16\%$ of the signal.

Thus about $0.65 \cdot 10^6$ combinations are selected. The $\bar{p}\pi^+$ effective mass distribution for the selected pairs of tracks is shown in Fig. 3. A clear signal of $\bar{\Lambda}^0$ decay (1) is seen in the spectrum. The background is caused mainly by combinations of reconstructed charged particles produced in the target ($\approx$ 40%), and in the air within the decay region ($\approx$ 60%). The spectrum is approximated

Table 1. Characteristics of antihyperon signals

Decay	Mass M_0, MeV/c^2	Resolution σ, MeV/c^2	Width Γ_R, MeV/c^2	Observed number
$\bar{\Lambda}^0 \to \bar{p}\pi^+$	1115.7 ± 0.3	1.4 ± 0.1	–	100300 ± 440
$\bar{\Xi}^+ \to \bar{\Lambda}^0\pi^+$	1321.8 ± 0.8	1.7 ± 0.1	–	1020 ± 40
$\bar{\Sigma}(1385)^- \to \bar{\Lambda}^0\pi^-$	1380.0 ± 1.4	–	31.7 ± 3.4	1760 ± 180
$\bar{\Sigma}(1385)^+ \to \bar{\Lambda}^0\pi^+$	1380.0 ± 2.1	–	35.9 ± 7.6	1180 ± 190

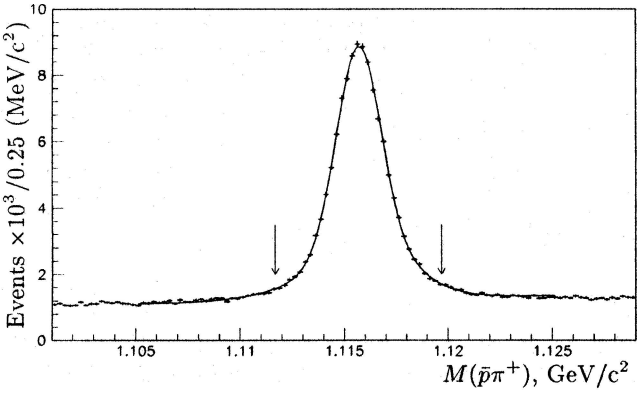

Fig. 3. Effective mass spectrum of $\bar{p}\pi^+$

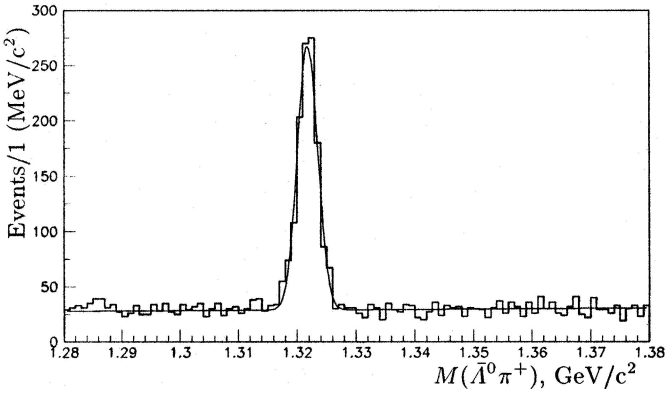

Fig. 4. Effective mass spectrum of $\bar{\Lambda}^0\pi^+$

using a MINUIT [21] minimisation routine by a sum of three Gaussian functions describing the signal and a linear function for the background. For a satisfactory quality of the fit (χ^2/ndf=1.2) at least three Gaussian functions are necessary because the experimental mass resolution depends on the $\bar{\Lambda}^0$ momentum. An average mass resolution $\sigma = 1.4$ MeV/c^2 is obtained as a root-mean-square of the three Gaussian widths weighted by the corresponding Gaussian amplitudes. An event is identified as a candidate to $\bar{\Lambda}^0$ decay if the effective mass $M(\bar{p}\pi^+)$ is within 4 MeV/c^2 (close to 3σ) from the nominal mass $M_{\bar{\Lambda}}$:

$$\left|M(\bar{p}\pi^+) - M_{\bar{\Lambda}}\right| < 4 \text{ MeV/c}^2. \tag{5}$$

The selected mass interval is marked with vertical arrows in Fig. 3.

These requirements leave about $0.14 \cdot 10^6$ candidates to the decay (1). The number of observed $\bar{\Lambda}^0$'s is calculated by integration of the Gaussian part of the approximating function, and equals $0.10 \cdot 10^6$. The number of background events is calculated by integration of the background function within the interval ± 4 MeV/c^2 from the nominal mass, and equals $0.04 \cdot 10^6$. Characteristics of the obtained $\bar{\Lambda}^0$ signal are presented in Table 1.

3.2 $\bar{\Xi}^+$ selection

The search for candidates to $\bar{\Xi}^+$ decay (2) is carried out by combining the $\bar{\Lambda}^0$ candidates with each of the additional positive tracks in the event. The CDA of the reconstructed $\bar{\Lambda}^0$ trajectory and the additional track should not exceed 0.5 cm. The point of their closest approach is considered as the decay vertex. To reduce the background caused by interactions in the target, it is required that the Z coordinate of the decay vertex $Z_{\bar{\Xi}}$ is situated at least 10 cm downstream the target:

$$Z_{\bar{\Xi}} - \left(Z_T + \frac{1}{2}L_T\right) > 10 \text{ cm}. \tag{6}$$

For further reduction of the background, it is required that the distance between $\bar{\Lambda}^0$ and $\bar{\Xi}^+$ decay vertices along the beam axis is greater than 5 cm:

$$Z_{\bar{\Lambda}} - Z_{\bar{\Xi}} > 5 \text{ cm}. \tag{7}$$

About $15 \cdot 10^3$ combinations survive these criteria. The $\bar{\Lambda}^0\pi^+$ effective mass spectrum of the selected combinations is shown in Fig. 4. A clear signal of $\bar{\Xi}^+$ decay (2) is seen in the spectrum. The spectrum is approximated by a sum of a Gaussian function describing the signal, and a linear function for the background. The number of observed decays is calculated by integration of the Gaussian term in the approximating function. Characteristics of the obtained $\bar{\Xi}^+$ signal are presented in Table 1.

3.3 $\bar{\Sigma}(1385)^{\pm}$ resonances selection

Candidates to the decays (3) of $\bar{\Sigma}(1385)^{\pm}$ are searched for in combinations of $\bar{\Lambda}^0$ candidates with each of the additional positive (negative) tracks. The CDA of the reconstructed $\bar{\Lambda}^0$ trajectory and the additional track should not exceed 0.2 cm. The point of closest approach of the $\bar{\Lambda}^0$ trajectory and the additional track is considered as the resonance decay vertex. The Z coordinate of the vertex $Z_{\bar{\Sigma}}$ should be situated within twice the experimental resolution ($\sigma_Z = 1$ cm) from the edges of the target:

$$|Z_{\bar{\Sigma}} - Z_T| < \frac{1}{2}L_T + 2\sigma_Z. \tag{8}$$

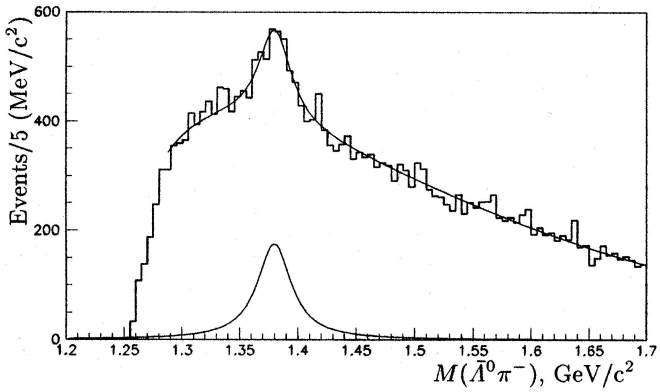

Fig. 5. Effective mass spectrum of $\bar{\Lambda}^0\pi^-$

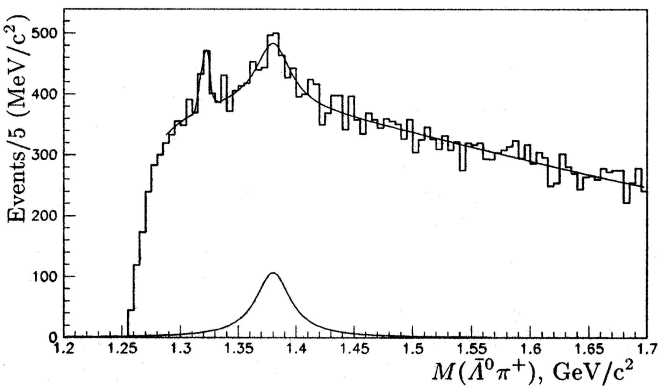

Fig. 6. Effective mass spectrum of $\bar{\Lambda}^0\pi^+$

About $33\cdot10^3$ combinations with a negative additional particle and $46\cdot10^3$ combinations with a positive additional particle have been selected. The effective mass spectra of $\bar{\Lambda}^0\pi^-$ and $\bar{\Lambda}^0\pi^+$ hypotheses for the selected combinations are shown in Fig. 5 and 6, respectively. Wide signals in these spectra correspond to the decays (3). The background is mainly combinatorial.

The spectra of $\bar{\Lambda}^0\pi^-$ and $\bar{\Lambda}^0\pi^+$ effective mass are approximated by the functions

$$\left(\frac{dN}{dM}\right)_- = BG(M) + BW(M), \tag{9}$$

and

$$\left(\frac{dN}{dM}\right)_+ = BG(M) + BW(M) + G(M), \tag{10}$$

respectively. Here the background, including the behaviour at the production threshold (M_{th}), is described by a smooth function

$$BG(M) = b_1(M - M_{th})^{b_2}\exp(b_3M + b_4M^2),\ M > M_{th}, \tag{11}$$

where b_1,..., b_4 are free parameters. The signal is approximated by the relativistic Breit-Wigner function

$$BW(M) = \frac{A\cdot M_0\cdot\Gamma_R\cdot M}{(M^2 - M_0^2)^2 + M_0^2\Gamma_R^2}, \tag{12}$$

where the free parameters are: A – scale factor, M_0 – position of the resonance maximum, and Γ_R – resonance width. The experimental mass resolution is significantly lower than resonance widths Γ_R. Therefore the obtained widths have not been corrected for mass resolution.

A Gaussian function $G(M)$ is added in the case of $\bar{\Sigma}(1385)^+$ to account for a peak in the spectrum due to $\bar{\Xi}^+ \to \bar{\Lambda}^0\pi^+$ decays occurring within or near the target (Fig. 6).

The amounts of detected resonance events are calculated by analytical integration of the Breit-Wigner terms in (9) and (10); the errors of the number of events are therefore obtained taking into account the errors of the parameters of the approximating functions. Characteristics of the $\bar{\Sigma}(1385)^\pm$ signals are presented in Table 1.

The measured masses of $\bar{\Lambda}^0$ and $\bar{\Xi}^+$ coincide within the errors with the nominal ones of the PDG [22]. The measured masses of $\bar{\Sigma}(1385)^\pm$ resonances are slightly lower than the nominal ones: the corresponding deviations are 2.8 MeV/c^2 for $\bar{\Sigma}(1385)^-$, and 7.2 MeV/c^2 for $\bar{\Sigma}(1385)^+$, and are caused by uncertainties in the value of magnetic field. The measured widths of the resonances are in agreement with the nominal ones.

4 Antihyperon production characteristics

Overall and differential acceptances have been calculated by a Monte-Carlo (MC) simulation. The events were generated in such a way that for each considered antihyperon $\bar{H}$ the corresponding hyperon H was chosen as an accompanying particle:

$$n + N \to \bar{H} + H + X. \tag{13}$$

Here X represents a set of accompanying particles generated by JETSET [23] in accordance with the conservation laws.

A GEANT based program [24] was used to trace the particles through the experimental setup. The simulated events were treated by the same reconstruction and analysis programs that were used to process the experimental data.

The inclusive production cross-section has been parametrised in the form

$$\frac{d^2\sigma}{dx_F dp_t^2} \sim (1 - |x_F|)^n\cdot\exp(-bp_t^2), \tag{14}$$

according to the quark counting rules [25,26]. Here $x_F = p_l^*/p_l^{max}$ is the Feynman variable, p_l^* is the longitudinal momentum of the produced particle, p_l^{max} is its maximum possible momentum (p_l^* and p_l^{max} are defined in neutron-nucleon centre of mass system), p_t is its transverse momentum.

Since the neutron beam is not monochromatic, the energy of the incident neutron is not known for each experimental event, and the value of x_F can not be obtained, in order to fit experimental distributions with (14). To

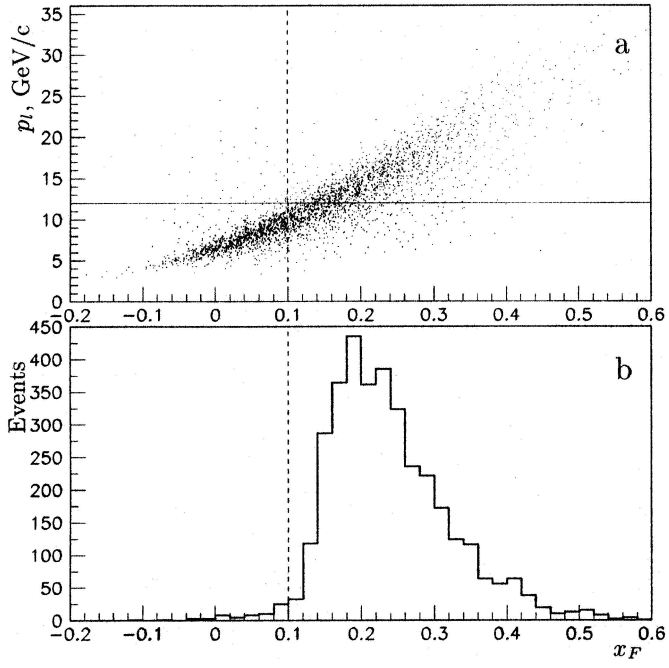

Fig. 7. **a** p_l vs x_F for simulated $\bar{\Lambda}^0$'s accepted by the applied conditions. $x_F^{\min}$=0.1, $p_l^{\min}$=12 GeV/c. **b** x_F distribution for events with $p_l > p_l^{\min}$

Table 2. Production parameters in the region $x_F > 0.1$

State	$p_l^{\min}$, GeV/c	n	b, $(\mathrm{GeV/c})^{-2}$
$\bar{\Lambda}^0$	12	8.0 ± 0.2	2.7 ± 0.1
$\bar{\Xi}^+$	13	7.5 ± 1.0	2.8 ± 0.3
$\bar{\Sigma}(1385)^-$	13	5.3 ± 0.3	2.4 ± 0.2
$\bar{\Sigma}(1385)^+$	14	5.0 ± 0.4	2.7 ± 0.2

estimate the values of the parameters n and b for the production of antihyperons by neutrons, p_l (longitudinal momentum in laboratory frame) and p_t^2 spectra of reconstructed antihyperons have been compared with those of simulated MC events. Each of the MC events has an incoming neutron energy generated according to the beam spectrum (Fig. 1), and the MC samples have been generated according to (14) for various values of n and b. The (p_l, p_t^2) distributions of MC events better matching the experimental ones are found on the basis of a χ^2 criterion, and the values of the parameters corresponding to the minimum χ^2 are selected. Errors of the parameters are evaluated in accordance with the method of multiparameter error calculation described in [21].

The differential cross-section parametrisation (14) is expected to be valid only at values of x_F corresponding to the fragmentation region, while in the central region the cross-section behaves differently. An appropriate cut in longitudinal momentum ($p_l > p_l^{\min}$) can be applied to experimental and MC generated events to ensure that both sets of events correspond to the values of x_F contained in a certain region $x_F > x_F^{\min}$. Figure 7 shows how the $p_l^{\min}$ boundary value can be chosen to select events with $x_F > x_F^{\min}$, for simulated $\bar{\Lambda}^0$ events. For $p_l^{\min} = 12$ GeV/c

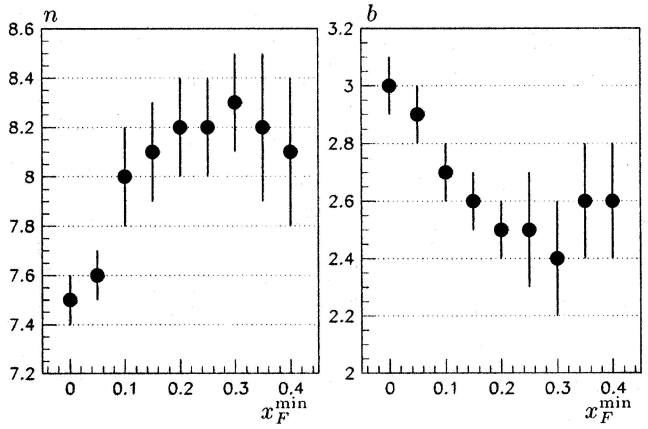

Fig. 8. $\bar{\Lambda}^0$ production parameters n and b at various $x_F^{\min}$

(solid line, Fig. 7a), almost all MC events with $p_l > p_l^{\min}$ have $x_F > x_F^{\min} = 0.1$ (dashed line), as seen in Fig.7b. The same selection applies also to experimental events.

By varying the $p_l^{\min}$ cut for $\bar{\Lambda}^0$ selection in order to span a $x_F^{\min}$ interval from 0 to 0.4 (in steps of 0.05), and performing the above procedure of matching MC samples generated at various values of n and b parameters to the experimental data, the estimated n and b values display a significant variation (Fig. 8) across the region $0 < x_F^{\min} < 0.4$, giving an indication of a change of regime around $x_F^{\min} = 0.1$, which might correspond to the point of transition from the central to the fragmentation region.

In order to minimise model dependence of the results, the determination of the parameters and cross-sections of antihyperon production has been carried out in the kinematic region of model validity (RMV). It was assumed that the RMV is defined by the condition $x_F > 0.1$ for all the studied antihyperons, which is in accordance with the result obtained for $\bar{\Lambda}^0$. The values of the $p_l^{\min}$ cut corresponding to the condition $x_F > 0.1$, production parameters (n and b) in the RMV, and their errors for each antihyperon under consideration are presented in Table 2. As an example, normalised experimental and simulated p_l and p_t^2 spectra of reconstructed $\bar{\Lambda}^0$ obtained in the RMV at minimal χ^2 are presented in Fig. 9. The spectra of the simulated events are in good agreement with the experimental ones.

A comparison of the obtained values of production parameters for $\bar{\Lambda}^0$ and $\bar{\Xi}^+$ with other experimental data obtained in nucleon-nucleon interactions in a wide energy range is presented in Fig. 10. It can be concluded that the production parameters are in agreement for antihyperon production by protons and neutrons, and are almost energy independent. The parameters of $\bar{\Sigma}(1385)^{\pm}$ production by nucleons have been measured for the first time.

5 Inclusive production cross-sections

5.1 Cross-sections in the region of model validity

Inclusive production cross-sections of antihyperons in the RMV are calculated by the formula

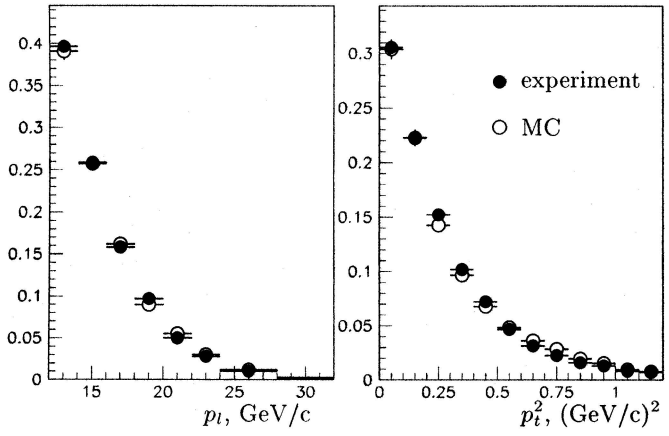

Fig. 9. Normalised p_l and p_t^2 spectra of $\bar{\Lambda}^0$ in the RMV for experimental and simulated events

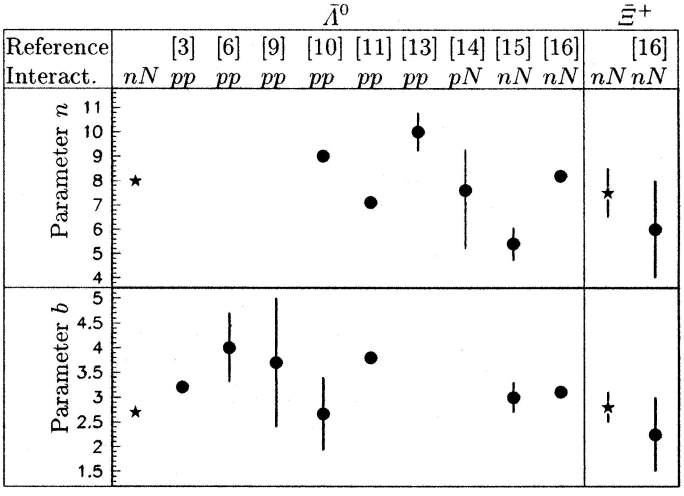

Fig. 10. Production parameters for $\bar{\Lambda}^0$ and $\bar{\Xi}^+$ in NN-interactions. The present results are marked with stars

$$\sigma_{nC} = \frac{N_s \cdot A}{M_n \cdot N_A \cdot L_T \cdot \varepsilon \cdot Br} , \qquad (15)$$

where N_s – the number of events in the signal; $A = 12$ – target nucleus atomic weight; $M_n = (2.43 \pm 0.08) \cdot 10^{11}$ – the number of neutrons that have passed through the target (neutron monitor); N_A – Avogadro constant; $L_T = 1.3$ g/cm^2 – target thickness; ε – overall efficiency of decay acceptance and selection; Br – branching ratio of a considered decay channel [22].

The number of the signal events N_s is defined as described in Sect. 3, but with an additional criterion on longitudinal momenta applied: $p_l > p_l^{\min}$. The efficiency ε is obtained from the MC simulation with the previously defined values of production parameters n and b. Event losses due to p_l cut, numbers of events in the remaining signal (N_s), and values of overall efficiency (ε) for the considered decays are presented in Table 3. Significant part of the rejected events are situated in the region $x_F > 0.1$ as well.

Calculated cross-sections of antihyperon inclusive production on carbon nuclei in the RMV are presented in Table 4. Statistical errors are caused by the errors of experimental signals, which are presented in Table 3. Systematic errors include uncertainties of the neutron monitor ($\delta M_n/M_n = 3.3\%$), overall efficiency ε, and decay branching ratio [22] combined in quadrature.

Table 3. Numbers of decays and efficiencies of registration

Decay	Loss at p_l cut	N_s	ε,%
$\bar{\Lambda}^0 \to \bar{p}\pi^+$	59%	41100 ± 290	2.28 ± 0.07
$\bar{\Sigma}(1385)^- \to \bar{\Lambda}^0\pi^-$	32%	1186 ± 179	0.91 ± 0.04
$\bar{\Sigma}(1385)^+ \to \bar{\Lambda}^0\pi^+$	30%	830 ± 275	0.79 ± 0.05
$\bar{\Xi}^+ \to \bar{\Lambda}^0\pi^+$	32%	724 ± 34	0.76 ± 0.05

Table 4. Cross-sections per carbon nucleus in region $x_F > 0.1$

State	σ_{nC}, μb				
$\bar{\Lambda}^0$	178.0	$\pm$	1.2 (stat)	$\pm$	8.3 (syst)
$\bar{\Sigma}(1385)^-$	14.6	$\pm$	2.2 (stat)	$\pm$	0.8 (syst)
$\bar{\Sigma}(1385)^+$	11.8	$\pm$	3.9 (stat)	$\pm$	0.8 (syst)
$\bar{\Xi}^+$	9.4	$\pm$	0.5 (stat)	$\pm$	0.6 (syst)

The error of efficiency is composed of a statistical error, which is the error of MC signal, and a systematic uncertainty. The latter is calculated as the variation of efficiency at various values of parameters n and b within their errors. For a cross-check the systematic error of efficiency was calculated as the variation of efficiency when the MC events were weighted independently in each p_l interval in order to vary the normalised p_l spectrum of accepted simulated events within the errors of the normalised experimental p_l spectrum. The two methods of error calculation obtain close results. The errors of ε presented in Table 3 are obtained as quadratic sums of statistical and systematic errors.

Systematic errors of cross-sections are dominated by the error of neutron monitor, and the systematic uncertainties of overall efficiency. Contributions of statistical errors of efficiency, and decay branching errors are negligible.

5.2 Extrapolation into the whole kinematic region

Our results were compared with the results of other experiments performed in proton and neutron beams, using the following relations for the total cross-sections of inclusive production for every considered antihyperon $\bar{H}$:

$$\sigma_{nN}(\bar{H}) \approx \sigma_{pN}(\bar{H}) \approx \sigma_{pp}(\bar{H}), \qquad (16)$$

based on the additive quark model.

The cross-sections σ_{nN} per nucleon have been obtained assuming $\sigma_{nC} = \sigma_{nN} \cdot A^{2/3}$, i.e. an A-dependence corresponding to a geometric nuclear cross-section, which is valid for soft processes at high x_F.

The extrapolation of cross-sections from the RMV into the whole kinematic region has been carried out under the assumption that the differential cross-section is a sym-

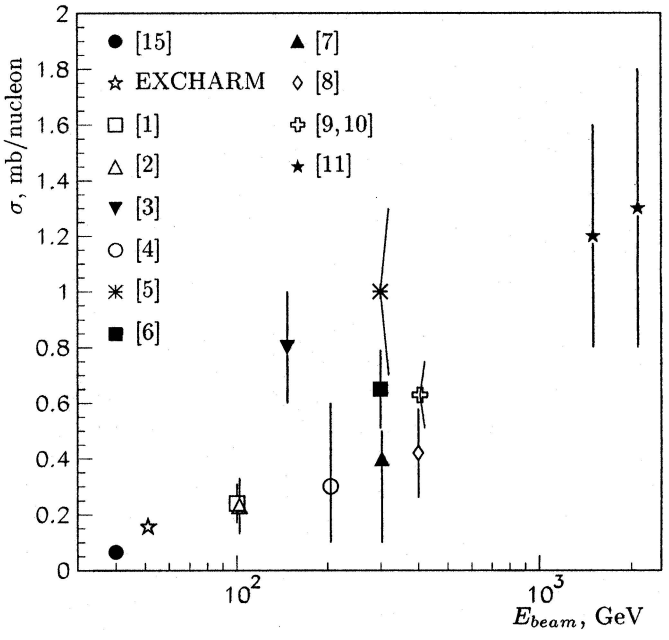

Fig. 11. Inclusive cross-sections of $\bar{\Lambda}^0$ production in NN-interactions

Table 5. Total cross-sections per nucleon

State	σ_{nN}, μb						
$\bar{\Lambda}^0$	154.0	$\pm$	1.0(stat)	$\pm$	7.2(syst)	$\pm$	18.0(ext)
$\bar{\Sigma}(1385)^-$	10.2	$\pm$	1.6(stat)	$\pm$	0.6(syst)	$\pm$	0.6(ext)
$\bar{\Sigma}(1385)^+$	8.2	$\pm$	2.8(stat)	$\pm$	0.6(syst)	$\pm$	0.5(ext)
$\bar{\Xi}^+$	7.9	$\pm$	0.4(stat)	$\pm$	0.5(syst)	$\pm$	0.9(ext)

metric function of x_F in the forward and backward hemispheres, as theoretically expected, and currently assumed.

In the central region $|x_F| < 0.1$, the differential cross-section (at least for $\bar{\Lambda}^0$ production) tends to increase for $|x_F| \to 0$ [3,9,12], though with a slope less steep [11] than implied by parametrisation (14), as apparent also in Fig. 8. Therefore the lower limit for total cross-section was determined under assumption that differential cross-section is a flat function of x_F in the region $|x_F| < 0.1$, and the upper limit was calculated assuming that the differential cross-section obeys the parametrisation (14) in this region. For $\bar{\Xi}^+$ and $\bar{\Sigma}(1385)^\pm$ the value of n in the region $|x_F| < 0.1$ used for the extrapolation was the same as that obtained in the RMV. For $\bar{\Lambda}^0$ the value $n = 7.5$ obtained for the lowest considered $x_F^{\min} = 0$ (and corresponding $p_l^{\min} = 8$ GeV/c) was used.

The extrapolated cross-sections per nucleon presented in Table 5 are average values of upper and lower limits. Extrapolation errors (ext) have been calculated as half of the difference between the two limits.

6 Summary

The inclusive production of $\bar{\Lambda}^0$, $\bar{\Xi}^+$, and $\bar{\Sigma}(1385)^\pm$ in nC-interactions at a mean neutron energy 51 GeV has been investigated. Differential cross-sections for these processes are compatible with the parametrisation of the quark counting model (14) in the kinematic region $x_F > 0.1$. The relevant parameters n and b were determined (Table 2). Their values for $\bar{\Lambda}^0$ and $\bar{\Xi}^+$ are in agreement with those obtained in other experiments, including the ones performed in proton beams. The parameters of $\bar{\Sigma}(1385)^\pm$ production by nucleons have been measured for the first time.

The inclusive cross-sections σ_{nC} in the region $x_F > 0.1$ have been determined (Table 4), as well as the corresponding cross-sections per nucleon σ_{nN}, which have been extrapolated into the whole kinematic region (Table 5). In Fig. 11 our results on the total $\bar{\Lambda}^0$ inclusive production cross-section per nucleon are compared with other results covering a wide energy range of pp and nN interactions: the present measurement is the most precise (statistic, systematic, and extrapolation errors are combined in quadrature), and agrees well with the overall trend of the data. Our results on $\bar{\Xi}^+$ and $\bar{\Sigma}(1385)^-$ inclusive production cross-sections also agree with the ones of [15] obtained in nC-interactions at 40 GeV mean neutron energy. The cross-section of $\bar{\Sigma}(1385)^+$ inclusive production by nucleons has been measured for the first time.

References

1. M. Alston et al., Phys. Rev. Lett. **35**, 142 (1975)
2. J.W. Chapman et al., Phys. Lett. **47** B, 465 (1973)
3. D. Brick et al., Nucl. Phys. B **164**, 1 (1980)
4. G. Charlton et al., Phys. Rev. Lett **30**, 574 (1973)
5. A. Sheng et al., Phys. Rev. D **11**, 1733 (1975)
6. F. LoPinto et al., Phys. Rev. D **22**, 573 (1980)
7. F.T. Dao et al., Phys. Rev. Lett. **30**, 1151 (1973)
8. R.D. Kass et al., Phys. Rev. D **20**, 605 (1979)
9. H. Kichimi et al., Phys. Lett. **72** B, 411 (1978)
10. H. Kichimi et al., Phys. Rev. D **20**, 37 (1979)
11. S. Erhan et al., Phys. Lett. **85** B, 447 (1979)
12. V. Blobel et al., Nucl. Phys. B **69**, 454 (1974)
13. M. Block et al., CERN-EP/79-82, 1979
14. R. Edwards et al., Phys. Rev. D **18**, 76 (1978)
15. A.N. Aleev et al., Yad. Fiz. **44**, 661 (1986)
16. M. Zavertyaev, Nucl. Phys. Proc. Suppl. B **93**, 62 (2001)
17. A.N. Aleev et al., *JINR P13-94-312* (Dubna 1994)
18. A.N. Aleev et al., Instrum. Exp. Tech. **42**, 481 (1999)
19. A. Boniushkina et al., *JINR P1-93-168* (Dubna 1993)
20. A.I. Zinchenko et al., *IFVE AN RK 92-01* (Alma-Ata 1992)
21. F. James, *Minuit Reference Manual*, D506 (CERN, 1994)
22. D.E. Groom et al., Eur. Phys. J. C **15**, 1 (2000)
23. T. Sjöstrand, Comp. Phys. Comm. **82**, 74 (1994)
24. G.A. Aralbaeva et al., *JINR P1-93-85* (Dubna 1993)
25. V.A. Matveev et al., Theor. Math. Phys. **40**, 778 (1979)
26. J.F. Gunion, Phys. Lett. **88** B, 150 (1979)